Two-Dimensional Trap for Ultrasensitive Quantification of Transient Protein Interactions

Oliver Beutel,[†] Friedrich Roder,[†] Oliver Birkholz,[†] Christian Rickert,[‡] Heinz-Jürgen Steinhoff,[‡] Michał Grzybek,[§,∥] Ünal Coskun,[§,∥] and Jacob Piehler*[,†]

[†]Department of Biology, University of Osnabrück, 49074 Osnabrück, Germany, [‡]Department of Physics, University of Osnabrück, 49076 Osnabrück, Germany, [§]Paul Langerhans Institute Dresden of the Helmholtz Centre Munich at the University Clinic Carl Gustav Carus TU Dresden, 01307 Dresden, Germany, and [∥]German Center for Diabetes Research (DZD), 85764 Neuherberg, Germany

ABSTRACT We present an ultrasensitive technique for quantitative protein–protein interaction analysis in a two-dimensional format based on phase-separated, micropatterned membranes. Interactions between proteins captured to lipid probes via an affinity tag trigger partitioning into the liquid-ordered phase, which is readily quantified by fluorescence imaging. Based on a calibration with well-defined low-affinity protein–protein interactions, equilibrium dissociation constants >1 mM were quantified. Direct capturing of proteins from mammalian cell lysates enabled us to detect homo- and heterodimerization of signal transducer and activator of transcription proteins. Using the epidermal growth factor receptor (EGFR) as a model system, quantification of low-affinity interactions between different receptor domains contributing to EGFR dimerization was achieved. By exploitation of specific features of the membrane-based assay, the regulation of EGFR dimerization by lipids was demonstrated.

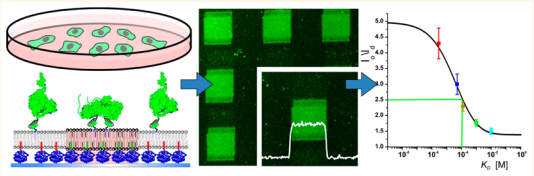

KEYWORDS: protein–protein interaction · polymer-supported membrane · lipid phase separation · fluorescence microscopy · signaling complexes · protein-lipid interaction

The spatiotemporal organization of biomolecules into functional supramolecular entities is mediated by a complex network of noncovalent interactions. A broad spectrum of techniques has been developed to probe protein–protein interactions *in vitro* and in living cells.[1] Popular techniques such as pull-down assays, the yeast-two-hybrid system,[2,3] bimolecular fluorescence complementation,[4,5] and other protein complementation techniques,[6,7] as well as protein arrays,[8−10] have contributed tremendously toward unraveling the protein interaction network of the cell. Complementary *in vitro* techniques such as real-time solid phase detection[11] and microscale thermophoresis[12] provide powerful means for validating protein–protein interactions in a quantitative manner. These techniques work very robustly for protein complexes with equilibrium dissociation constants (K_D) of up to a few micromolar. Reliable quantification of much weaker interactions, however, remains challenging, because high protein concentrations (in the range of the K_D) are required, which often are very difficult to produce and which increase the background signals of traditional detection techniques. Moreover, low affinity interactions are accompanied by short complex lifetimes (<1 s), which are very challenging to resolve by kinetic detection techniques. Typically, isothermal titration calorimetry[13,14] or analytical ultracentrifugation[15] are used for determining the equilibrium constants of such low-affinity interactions, methods that require large amounts of highly purified proteins. Even for isothermal titration calorimetry, transient protein homodimerization remains particularly challenging, since separation of the interaction partners is not possible.

Low-affinity, highly transient protein interactions are particularly relevant in the context of membranes, where high local concentrations promote efficient complex formation. Here, we have exploited this concept for quantitative protein–protein interaction analysis in a two-dimensional format. For this purpose, polymer-supported membranes (PSM) were employed as a

* Address correspondence to piehler@uos.de.

Received for review May 5, 2015 and accepted September 2, 2015.

Published online September 02, 2015
10.1021/acsnano.5b02696

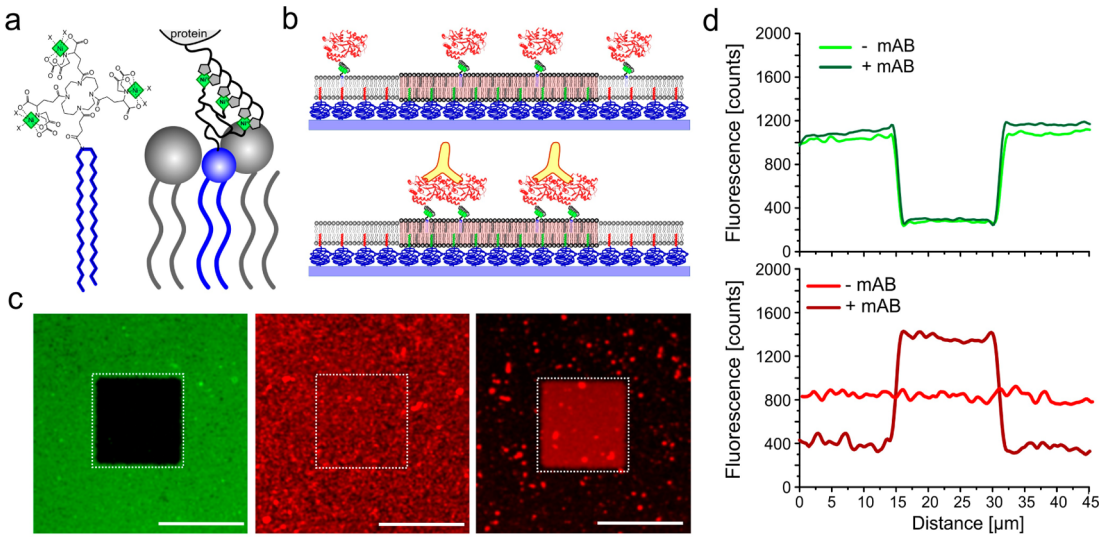

Figure 1. Concept and validation of the two-dimensional protein interaction trap (2DTrap). (a, b) Principle of the assay: monomeric proteins tethered to PSMs via tris-NTA−DODA (a) are homogeneously distributed in phase-separated lipid membranes and partition into the l_o-phase upon dimerization (b). (c, d) Proof of concept experiment with ^{Cy5}MBP-H6 captured to micropatterned phase-separated PSM doped with tris-NTA−DODA. (c) Fluorescence images of an l_d phase marker (green channel) and ^{Cy5}MBP-H6 before (center image) and after addition of 20 nM of a monoclonal anti-MBP antibody (right image). Scale bars 20 μm. (d) Comparison of the fluorescence intensity profiles of the l_d phase marker (top) and the ^{Cy5}MBP-H6 (bottom) before and after addition of an anti-MBP antibody (mAB).

spatially and temporally addressable, highly versatile analytical platform.[16−19] Interactions between proteins tethered to PSM were quantified via partitioning between liquid disordered (l_d) and liquid-ordered (l_o) lipid phases. For protein capturing, the PSM was doped with tris(nitrilo triacetic acid) (tris-NTA) conjugated to dioctadecylamine (tris-NTA−DODA, Figure 1a), which binds His-tagged proteins with high affinity and defined stoichiometry.[20] Tris-NTA−DODA complexed with three Ni(II) ions is approximately equally distributed between l_o and l_d phase when bound to a hexahistidine (H6)-tagged protein, yet efficiently partitions into the l_o phase upon cross-linking by means of elongated oligohistidine-tags (*e.g.*, H10).[21] We exploited this two-dimensional trapping (2DTrap) of protein complexes into l_o domains as a quantitative readout for dimerization of membrane-tethered proteins, which can be readily visualized within micrometer dimensions. For reliable and automated quantification of lipid phase partitioning, we employed membranes supported by a poly(ethylene glycol) polymer brush with a binary micropattern comprising palmitic and oleic acid tethers.[22] Thus, polymer-supported membranes (PSM) with micropatterned l_o phases were obtained, which allow robust quantification of phase partitioning (Figure 1b). Efficient capturing of fluorescence-labeled, hexahistidine-tagged target proteins to these phase-separated, micropatterned PSMs doped with tris-NTA−DODA allows us to achieve local protein concentrations that are sufficient for measurements of low binding affinities and to directly quantify the equilibrium constant from the distribution between l_o and l_d phases.

RESULTS AND DISCUSSION

As a proof-of-concept experiment for detecting and quantifying protein interactions by 2DTrap, antibody-mediated dimerization of a model protein was investigated. To this end, Cy5-labeled maltose binding protein (MBP) fused to a hexahistidine tag (^{Cy5}MBP-H6) was captured to a micropatterned membrane prepared from a lipid mixture comprising 1,2-dioleoyl-*sn*-glycero-3-phosphocholine (DOPC, 42 mol %), sphingomyelin (SM, 28 mol %), and cholesterol (28 mol %), which was doped with 1 mol % tris-NTA−DODA and 0.1−0.2 mol % fluorescent l_d marker. With this composition from uncharged and zwitterionic lipids, preferential orientation of tethered proteins due to electrostatic interactions can be excluded. To furthermore ensure quasi-three-dimensional interaction of membrane-tethered proteins, we employed peptide linkers of nine or more amino acid residues between the protein and the His-tag. Molecular dynamics simulations confirmed that this linker length is sufficient for proteins to randomly explore the entire spectrum of dihedral angles with respect to the membrane plane as required for the encounter of interaction partners in all possible relative orientations (Supporting Figure S2). Dimerization was induced by addition of a monoclonal anti-MBP immunoglobulin G (Figure 1b,c and Supporting Figure S1). Owing to its bivalency, this monoclonal antibody (mAb) can simultaneously bind two MBP molecules as schematically depicted in Figure 1b. Upon incubation of the anti-MBP mAb, partitioning of tris-NTA−DODA-anchored ^{Cy5}MBP-H6 between the l_o and the l_d phases increased from ~1:1 to

~4:1 (Figure 1c,d and Supporting Video 1). Unchanged partitioning of an l_d marker during MBP dimerization confirmed that the change in contrast was caused by change in partitioning of the tris-NTA−DODA-anchored ^{Cy5}MBP-H6 rather than by alterations in the lipid phase properties. Since a monoclonal antibody was applied, which binds only to a single epitope of MBP, strict protein dimerization was ensured, thus confirming that dimerization of tris-NTA−DODA-anchored proteins can be detected by increased l_o phase partitioning. Very similar partitioning as for mAb-dimerized mMBP-H6 was observed for different proteins with longer His-tags (H10−H14, Supporting Figure S3), which we have previously shown to efficiently cross-link tris-NTA−DODA.[21] Because the minimum and maximum partitioning values varied for PSM assembled on different micropatterned substrates, mAb-induced MBP dimerization was performed in each case for a reliable calibration.

While convenient intensity-based readout was achieved by using micropatterned, phase-separated PSM, we also exploited the different diffusion properties of tris-NTA−DODA in l_o and l_d phases for quantification of phase partitioning. For quantification of protein mobility, we employed single molecule tracking. ^{Cy5}MBP-H6 was tethered onto phase-separated, micopatterned PSM at a concentration of ~2 molecules/μm^2 and imaged by time-lapse single molecule total internal reflection fluorescence microscopy before (Figure 2a) and after addition of the anti-MBP mAb (Figure 2b). A bimodal distribution of diffusion constants was obtained from single trajectory analysis, corresponding to their localization in either l_o ($D \approx 0.1$ μm^2/s) or l_d ($D \approx 1$ μm^2/s) domains (Figure 2c). Indeed, sorting trajectories into slow and fast diffusing species highly correlated with the phase-separated l_o/l_d pattern. Thus, lipid phase partitioning could be directly quantified from the distribution of diffusion constants. Upon application of the anti-MBP mAb, partitioning into the l_o phase, as judged from the diffusion properties, was increased from 1:1 to 5:1 (Figure 2d). Importantly, the same l_o/l_d partitioning behavior of monomeric and dimeric ^{Cy5}MBP-H6 was obtained by this diffusion-based analysis compared with the spatial evaluation based on the micropattern geometry.

In order to explore the capability to probe low affinity protein interactions by 2DTrap, we employed the enhanced green fluorescent protein (EGFP), which dimerizes head-to-tail with an estimated K_D of ~0.1 mM.[23] The A206K mutation within the monomeric EGFP (mEGFP) increases the K_D to ~70 mM.[23] Strikingly, strong partitioning of purified EGFP fused to an N-terminal H6-tag (H6-EGFP) into the l_o phase was observed upon tethering to phase-separated PSM (Figure 3a). Much lower partitioning into the l_o-phase was observed for H6-mEGFP, while the monomeric H6-tagged HaloTag protein[24] labeled with TMR (^{TMR}HaloTag-H6) did not show any increase in

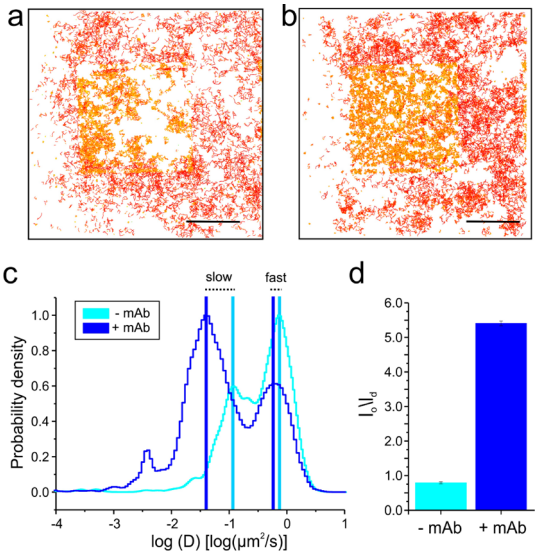

Figure 2. Phase partitioning quantified by single molecule tracking. (a, b) Trajectories of individual ^{Cy5}MBP-H6 before (a) and after (b) dimerization by an anti-MBP mAB, color-coded according to their diffusion kinetics (yellow, slow; red, fast). Scale bars 10 μm. (c) Distribution of diffusion constants of monomeric and dimerized ^{Cy5}MBP-H6 tethered to micropatterned phase-separated membranes. Diffusion constant of 2500 trajectories with a minimum length of 160 ms (>5 frames) before and after AB were evaluated. Note that the shifts in the maxima are caused by the reduced mobility upon dimerization. (d) Partitioning before and after application of the anti-MBP mAB as obtained from three independent experiments by counting fast and slow moving particles (error bars indicate the standard errors of the mean). After counting the slow and fast particles, l_o/l_d partitioning ratios of 0.8 ± 0.1 before and 5.5 ± 0.25 after addition of mAB were observed.

contrast (Figure 3a). Since the monomer−dimer equilibrium on the membrane is expected to depend on the protein surface concentration, we probed l_o/l_d partitioning at different loading of H6-EGFP, H6-mEGFP, and ^{TMR}HaloTag-H6, respectively. The absolute surface concentrations obtained were quantified by label-free detection (Supporting Figure S4) in order to yield a quantitative, surface concentration-dependent concentration−dimerization relationship (Figure 3a), which could be fitted by a comprehensive model of this process based on the law of mass action (Figure 3a and Supporting Results). In order to further enhance the sensitivity, robustness, and versatility of direct protein capturing, we preloaded the membrane with a commercial, H6-tagged anti-GFP nanobody,[25] a cameloid-derived monovalent single-chain antibody fragment. This nanobody quasi-irreversibly binds mEGFP much faster ($k_a = 5 \times 10^6$ M^{-1} s^{-1}) compared with the tris-NTA/oligohistidine interaction (5×10^5 M^{-1} s^{-1}), thus allowing even more rapid protein capturing and thus more defined and reproducible loading of the membrane (Supporting Figure S5). Indeed, very similar partitioning of mEGFP and EGFP was observed for capture via the nanbody compared with His-tag-specific capturing (Supporting Figure S6), confirming the robustness of the assay.

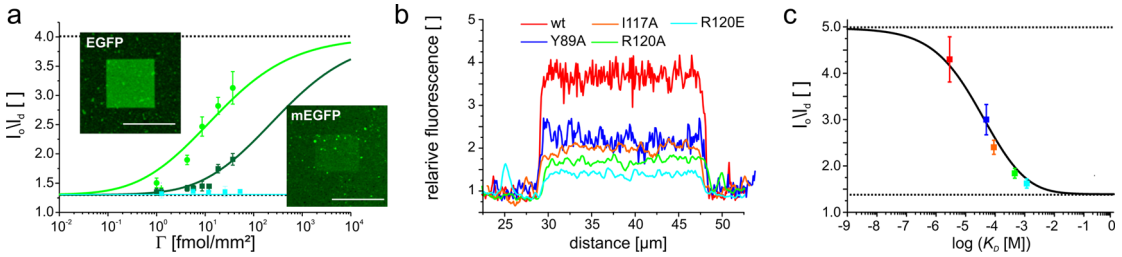

Figure 3. Calibration of the 2DTrap assay. (a) Relative partitioning of H6-EGFP (light green), H6-mEGFP (dark green), and ^{TMR}HaloTag-H6 (cyan) tethered to phase-separated membranes at different surface concentrations. The curves were fitted by a comprehensive model describing dimerization and partitioning based on the law of mass action (Supporting Results). Minimum and maximum contrast was fixed based on the calibration with MBP (dotted lines). Representative raw images of H6-EGFP and H6-mEGFP at corresponding concentrations are shown in the inset. Scale bars 20 μm. (b, c) Calibration of the assays based on ligand-induced dimerization of type I interferon receptor. (b) Partitioning of labeled IFNα2 WT and different mutants upon binding to IFNAR1-H6 and IFNAR2-H6 captured to micropatterned phase-separated membranes. Intensity profiles obtained from images shown in Supporting Figure S7 are shown. (c) I_o/I_d ratio as a function of 3D K_D (same color coding as in panel b) and calibration curve obtained by fitting the model.

For calibrating the 2DTrap assay with respect to binding affinities, we employed a well-characterized model system based on ligand-induced heterodimerization of the type I interferon (IFN) receptor subunits IFNAR1 and IFNAR2.[26] The ectodomains of these proteins fused to a C-terminal H6-tag were tethered onto micropatterned, phase-separated PSM. Since IFNα2 binds IFNAR2 with high affinity (K_D = 5 nM), dimerization on the membrane is determined by its low affinity toward IFNAR1 (K_D = 5 μM for wild-type IFNα2).[26] For calibration, we employed wild-type IFNα2 and mutants with different binding affinities toward IFNAR1,[27,28] which were site-specifically labeled with DY647.[29] Upon addition of labeled wild-type IFNα2, maximum I_o/I_d partitioning was observed (Supporting Figure S7 and Figure 3b). In contrast, reduced I_o/I_d partitioning was observed for IFNα2 mutants with reduced IFNAR1 binding affinities. These were, in parallel, quantified by simultaneous total internal reflection fluorescence spectroscopy and reflectance interference detection,[30] covering a spectrum of equilibrium dissociation constants from 1 μM to 1 mM (Supporting Figure S8 and Supporting Table S1). Plotting I_o/I_d phase partitioning vs K_D yielded a calibration curve, which could be fitted by a comprehensive binding and partitioning model. This model comprises four equilibrium constants describing the monomer−dimer equilibrium in I_d (K_1) and I_o (K_2) phases, respectively, as well as partitioning of monomer (K_3) and dimer (K_4) into both phases (details provided as Supporting Results). By fitting this model to the calibration data, we determined a conversion factor from 2D into 3D K_D values (Supporting Table S1). At the chosen surface concentration of 0.5 ng/mm^2 corresponding to 10 fmol/mm^2, an accessible range of binding affinities between 1 μM and 1 mM was obtained (Figure 3c). Applying this calibration curve to the contrast observed for H6-EGFP (Figure 3a), a K_D value of 110 ± 10 μM was obtained, which is in very good agreement with previously published data.[23] For mCherry as a potential fluorescent tag for probing protein heterodimerization, a similar K_D as for EGFP was obtained (~100 μM, Supporting Figure S9). Because this intrinsic dimerization affinity of mCherry is too high for unbiased interaction assays, we used the HaloTag for spectrally distinct fluorescence labeling because this protein is strictly monomeric and can be *in situ* conjugated with different fluorescent dyes (Figure 3a and Supporting Figure S9).

Because 2DTrap assays require only minute protein quantities, we tested protein capturing to membranes directly from cleared cell lysates (Supporting Figure S10). Upon incubating lysates from *E. coli* expressing H6-EGFP and H6-mEGFP, respectively, the I_o/I_d phase partitioning observed for purified H6-EGFP and H6-mEGFP were very well reproduced (Supporting Figure S11), confirming robust dimerization analysis from cell lysates. As a model system for homo- and heterodimerization of protein directly captured from mammalian cell lysates, we explored the interaction between the signal transducer and activator of transcription (STAT) proteins STAT1 and STAT2. These proteins are important effector proteins in signaling transduction by cytokine receptors, which form various homo- and heterodimeric transcription factors upon tyrosine phosphorylation.[31] STAT1 was demonstrated to constitutively (i.e., independently of phosphorylation) homodimerize with a K_D of 50 nM.[32] In contrast, STAT2 was suggested to interact with STAT1[33] but not to homodimerize, though these interactions have not been verified in detail. Here, we tested these interactions by the 2D phase partitioning assay using direct capturing of H6-tagged proteins transiently expressed in HEK 293 cells. Cleared cell lysates from cells expressing STAT1 fused to mEGFP and a His-tag (STAT1−mEGFP-H6) were exposed to phase-separated membranes, and high partitioning into I_o-phases could be observed (Figure 4a) as expected for homodimerization. In contrast, no partitioning beyond the background was observed for tetramethylrhodamine-labeled STAT2 fused to the HaloTag and a His-tag (STAT2−HaloTag^{TMR}-H6), confirming that STAT2 does

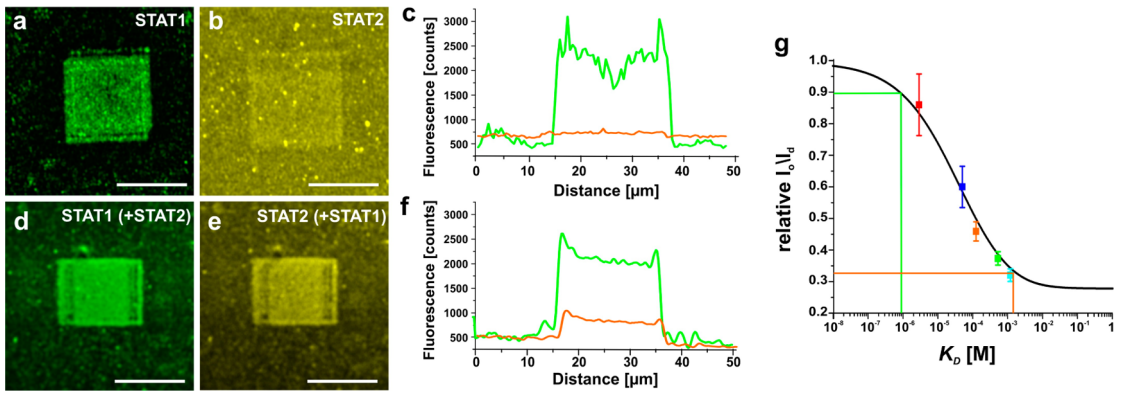

Figure 4. Homo- and heterodimerization of STAT1 and STAT2 detected by 2DTrap with cell lysates. (a–c) Partitioning of STAT1–mEGFP-H6 (a) or STAT2–HaloTag^{TMR}-H6 (b) captured to micropatterned phase-separated PSM and comparison of the intensity profiles (c). (d–f) Partitioning of STAT1–mEGFP-H6 (d) and STAT2–HaloTag^{TMR}-H6 (e) cocaptured to micropatterned phase-separated PSM and comparison of the intensity profiles (f). (g) Binding affinities estimated for STAT1 and STAT2 homo- and heterodimerization.

not homodimerize. Upon cocapture of STAT1–mEGFP-H6 and STAT2–HaloTag^{TMR}-H6 in a 1:1 ratio to the membrane, however, significant partitioning of both STAT1 and STAT2 into the l_o phase was observed (Figure 4d–f). These results corroborate that STAT1 constitutively homodimerizes and heterodimerizes with STAT2, in good agreement to previous reports.[32−34]

Since 2DTrap is particularly powerful for studying low affinity interactions in the context of membranes, we applied it for quantifying critical interactions involved in the dimerization of the epidermal growth factor receptor (EGFR), a key regulator in cell proliferation and differentiation. Aberrant activation of EGFR is directly implicated in the pathogenesis and progression of different cancers.[35] Interactions between the kinase domains of the EGFR have been suggested to play an important role in receptor dimerization and activation.[36,37] The juxtamembrane segment A (JM-A) located between the kinase domain and the transmembrane segment has been shown to substantially promote dimerization of the kinase domains and is believed to act as an allosteric regulator of EGFR activity.[36−38] To quantify these interactions, the EGFR kinase domains with and without the JM-A domain fused to N-terminal H6 and mEGFP were transiently expressed in HEK293 cells and thereon captured onto phase-separated PSM directly from cleared cell lysates (Figure 5a,b). Dimerization was observed for both kinase variants but with marked differences in the binding affinities (Figure 5c,d): while relatively high affinity ($K_D \approx 1\ \mu M$) dimerization was observed in the presence of the JM-A domain, a K_D of 750 μM was obtained for the EGFR kinase domain without JM-A (Figure 5d), in agreement with previous data.[37] Thus, we could for the first time directly detect and quantify very weak dimerization of the EGFR kinase domain.

Protein conformations and interactions at membranes are frequently regulated by protein–lipid interactions,[39] which are extremely difficult to assess directly.

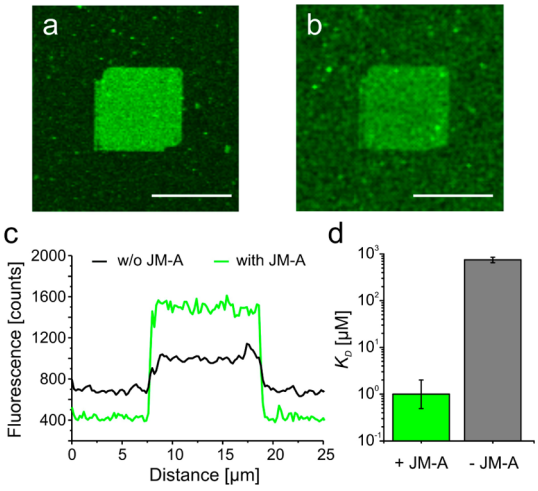

Figure 5. Quantification of EGFR kinase domain dimerization by 2DTrap assays with cell lysates. (a, b) Confocal images of H6-tagged EGFR kinase domain with (a) and without (b) the JM-A segment tethered to micropatterned membranes. Scale bars 10 μm. (c) Intensity profile of the patterns shown in panels a and b. (d) Binding affinities obtained from three independent experiments for the EGFR kinase domain with (1 ± 1 μM) and without (750 ± 100 μM) JM-A segment.

A prominent example is the ligand-induced dimerization of the EGFR ectodomains. The monosialodihexosylganglioside (GM3) has been previously suggested to stabilize the monomeric form of the full length EGFR and thus to attenuate kinase domain activation, without perturbing the ligand binding properties of the receptor.[40,41] Using this interaction as a model system, we tested the compatibility of the membrane-based 2DTrap assay for systematically studying regulation of protein interactions by lipids. For this purpose, EGFR ectodomain fused to a C-terminal H6-tag was produced in insect cells and was site-specifically labeled with DY647 *via* an N-terminal ybbR-tag (^{DY647}EGFR-H6). In the absence of ligand, dimerization of membrane-tethered ^{DY647}EGFR-H6 could be detected only at very high surface concentrations ($K_D \approx 10$ mM, Figure 6a

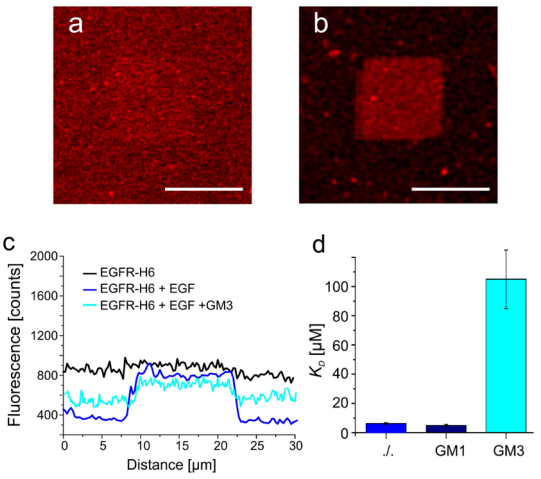

Figure 6. 2DTrap quantification of EGFR-ectodomain dimerization and its regulation by lipids. (a, b) Confocal image of ^{DY647}EGFR-H6 tethered to micropatterned membranes before (a) and after (b) addition of 1 μM EGF. (c, d) Intensity profiles (c) and equilibrium dissociation constants, K_D (d), obtained from the assay. The equilibrium dissociation constants for the EGFR-H6 homodimerization after EGF addition (6.2 $\pm$ 0.6 μM) and in the presence of GM1 (4.9 $\pm$ 0.7 μM) or GM3 (105 $\pm$ 20 μM) were obtained from three independent experiments.

and Supporting Figure S12). After addition of EGF, efficient partitioning into the l_o phase was observed (Figure 6b and Supporting Video 2) confirming ligand-induced dimerization of the extracellular domains. A $K_D \approx 5$ μM was obtained for EGFR-H6 homodimerization (Figure 6c,d), in good agreement with solution phase measurements by ITC.[42] Interestingly, for membranes doped with GM3, which was homogeneously distributed in both lipid phases (Supporting Figure S13), EGF-induced dimerization was very strongly reduced (K_D = 105 $\pm$ 20 μM, Figure 6c,d and Supporting Table S2), while efficient dimerization by a monoclonal antibody could still be observed (Supporting Figure S14). In case of GM1, EGF-induced dimerization was not affected (Figure 6d and Supporting Figure S14), confirming that GM3 indeed specifically interferes with EGF-mediated interaction between the EGFR ectodomains.[40] While the inhibition of EGFR by GM3 with respect to allosteric kinase domain inhibition has been described recently,[41] these experiments for the first time directly show the critical role of GM3 in ligand-dependent EGFR dimerization.

CONCLUSIONS

We have here developed 2DTrap as a simple, robust, and versatile method for quantifying low-affinity protein interactions requiring minute amounts and concentrations of target proteins. This was achieved by implementing a novel concept for detecting protein interactions within a two-dimensional fluid, which exploits altered lipid phase-partitioning upon complex formation. With the simple implementation of the assay used here, binding affinities up to 1 mM were assessed with proteins directly captured from cell lysates. However, by increase of the surface concentration of tethered proteins, for example, by higher doping with tris-NTA, and improved membrane capturing (*e.g.*, *via* the anti-GFP nanobody) even lower affinities are accessible. Thus, also a simple and robust control of surface concentrations could be achieved, which are important for reliable quantification of binding affinities. For quantification of high affinity interactions, which requires substantially reduced surface concentrations, we developed a single molecule tracking-based readout taking advantage of the differential diffusion properties in l_o and l_d domains.

The 2DTrap assay turned out to be robust as binding affinities of protein complexes with different size, structure, and relative orientation of the interaction partners could be reliably reproduced (Supporting Table S3). This was achieved by the orientationally highly flexible attachment to the membrane *via* a peptide linker, which ensures quasi-three-dimensional behavior of the membrane-tethered proteins. Here, femtomole protein quantities were required due to macroscopic sample handling, yet only 10000 protein molecules are actually sufficient for quantification because the readout is obtained from an area of 50 $\times$ 50 μm^2. By exploitation of more efficient protein capturing, for example, *via* the anti-GFP nanobody, in combination with microfluidic cell handling, quantitative interaction analysis at the single cell level therefore can be envisaged. With this high potential for miniaturization and parallelization, 2DTrap will be particularly powerful for screening the subtle contributions of protein domains for assembly of macromolecular complexes in a quantitative manner. Furthermore, the 2DTrap assay opens exciting possibilities to systematically explore the regulatory role of lipid–protein interactions at the membrane, such as the attenuation of EGFR dimerization by GM3 demonstrated here. By inclusion of charged lipids, unraveling the role of protein orientation caused by electrostatic interactions with the membrane can be envisaged. Taken together, 2DTrap appears to be a versatile approach to quantify low affinity protein–protein and protein–lipid interactions.

METHODS

Materials. Materials and methods describing the production and labeling of proteins in bacterial, insect, and mammalian cells, as well as surface-sensitive detection and molecular dynamics simulations, are provided as Supporting Methods.

Surface Patterning. Surface chemistry was carried out on standard glass cover slides for fluorescence microscopy. Surface coating with a thin PEG polymer brush and further micropatterned functionalization with fatty acid groups was carried out as described in detail previously.[22,43] Briefly, cleaned substrate

surfaces were reacted with pure (3-glycidyloxypropyl)trimethoxysilane followed by coupling of molten diamino-PEG for 4 h at 75 °C. Surface amine groups were caged by incubation with 6-nitroveratryl chloroformate and uncaged by irradiation through a photomask for 2 min using a 75 W xenon lamp equipped with a 280−400 nm dichroic mirror. After reacting deprotected amine groups with palmitic acid, the surface was again irradiated as before but without a photomask, and the remaining surface amines were reacted with oleic acid. In order to ensure optimum lipid phase patterning, a photomask was used yielding a micropattern with a surface area ratio between palmitic and oleic acid of ∼1:3, corresponding to the ratio observed for spontaneous l_o/l_d phase separation of the lipid mixture in nonpatterned PSM.

Vesicle Preparation and Assembly of Micropatterned PSM. DOPC, SM, and cholesterol were mixed in chloroform at a molar ratio of DOPC/SM/cholesterol = 30:35:35, and 0.1−0.2 mol % of the fluorescent lipid bovine heart phosphatidylcholine or DiD was added. After removal of the solvent and hydration of the lipid film in HBS (20 mM Hepes, 150 mM NaCl, pH 7.5), the solution was intensively sonicated three times for 5 min cooled only by a water bath in order to obtain small unilamellar vesicles (SUV). Tris-NTA−DODA was incorporated by mixing vesicles with DOPC doped with 5 mol % tris-NTA−DODA with a ternary mixture of DOPC/SM/cholesterol = 30:35:35 in a ratio of 1:5. For assembly of a PSM, vesicles were incubated on micropatterned substrates for 10 min. Unbound vesicles were washed off, and fusion was induced by incubation with a 10% (w/v) PEG solution for 10−20 min.[22,43] Heating to 60 °C and slow cooling to room temperature was applied to improve separation of lipid phases into micropatterns. Excessive material was washed off the bilayer by intensive pipetting of HBS. In order to bind His-tagged proteins, the surface was sequentially rinsed with 250 mM imidazole and 50 mM EDTA and then incubated with 50 mM $NiCl_2$ in HBS for 10 min. Subsequently, the surface was extensively rinsed with HBS buffer in order to remove excess Ni(II) ions and then incubated with His-tagged proteins (100 nM if not stated otherwise) for 5 min. Unbound protein was subsequently removed by carefully rinsing with HBS.

Confocal Imaging. Confocal imaging and photobleaching background measurement were carried out with a confocal laser-scanning microscope (Olympus FluoView 1000) equipped with a multiline argon laser (458/488/515 nm) and laser diodes of 405, 559 and 635 nm as well as spectral detectors. BODIPY-FL 1,2-dihexadecanoyl-*sn*-glycero-3-phosphoethanolamine (DHPE), EGFP, mEGFP, ^{AF488}MBP-H6, and ^{AF488}EGFR-H6 were excited with 5−25 μW at 488 nm, and fluorescence emission between 500 and 600 nm was detected. DiD and ^{DY647}MBP-H6 were excited with 5−25 μW at 635 nm, and fluorescence was detected between 650 and 750 nm. mCherry was excited with 5−25 μW at 559 nm, and fluorescence was detected between 565 and 620 nm. The laser output power was measured at the objective. Micropatterned, phase-separated PSMs were prepared in an open incubation chamber and loaded with His-tagged proteins as described above. The partitioning of membrane-bound proteins was quantified by the fluorescence intensity ratio of the l_o (I_{l_o}) and the l_d (I_{l_d}) phases, which were corrected for background intensity (I_{bg}).[44,45]

$$l_o/l_d = \frac{I_{l_o} - I_{bg}}{I_{l_d} - I_{bg}} \quad (1)$$

Average fluorescence intensities from nine micropatterned regions (individual squares per experiment) within l_o and l_d phases, respectively, were quantified using ImageJ. The background intensities (I_{bg}) were measured after photobleaching these regions. For determination of the K_D, the l_o/l_d ratio based on the calibration was normalized to the minimum and maximum l_o/l_d partitioning of the micropatterned membrane. For quantifying these values, partitioning of ^{DY647}MBP-H6 in the absence (minimum boundary) and in the presence of 20 nM monoclonal anti-MBP mAb (maximum boundary) was experimentally determined for each micropatterned support.

For calibration, H6-tagged IFN receptor subunits IFNAR1 and IFNAR2 were tethered to the membrane in a 1:1 ratio. By using fluorescence-labeled IFNα2 mutants with different affinities toward IFNAR 1, we obtained a calibration curve by measuring the l_o/l_d ratio. The K_D values of the IFN mutants, which were quantified by ligand dissociation kinetics using TIRFS-RIf detection (see Supplementary Methods),[30] were plotted against the l_o/l_d ratio and fitted by eq S8 (Supplementary Results) to obtain the calibration curve. The calibration curve was used to calculate equilibrium constants from l_o/l_d ratios obtained for different proteins of interest.

Single Molecule Imaging and Image Analysis. Single molecule tracking experiments were carried out by total internal reflection fluorescence microscopy with an inverted microscope (Olympus IX71) equipped with a single-line total internal reflection (TIR) illumination condenser (Olympus) and a back-illuminated electron multiplied CCD camera (iXon DU897D, 512 × 512 pixel from Andor Technology). A 150× magnification objective with a numerical aperture of 1.45 (UAPO 150×/1.45 TIRFM, Olympus) was employed for TIR illumination of the sample. Total internal reflection fluorescence imaging was carried out with the 647 nm line of an argon−krypton laser for excitation operated at an output power of ∼1 mW at the objective. Fluorescence was detected using a 690/70 band-pass filter (Chroma). Images were acquired with a time resolution of 16 ms/frame. All experiments were carried out using buffer complemented with oxygen scavenger and a redox-active photoprotectant [0.5 mg/mL glucose oxidase (Sigma), 0.04 mg/mL catalase (Roche AppliedScience), 5% w/v glucose, 1 μM ascorbic acid, and 1 μM methyl viologene] to minimize photobleaching.[46] The multitarget tracking (MTT)[47] algorithm was used to localize and track individual fluorescent molecules. Before the particle positions were handed over to the tracking algorithm, immobile particles were removed by density-based spatial clustering of applications with noise filtering,[48] which identified clusters by exploiting a spatiotemporal correlation of immobile signals. The diffusion histograms were obtained by fitting the first five steps of the mean square displacement of each trajectory with a free diffusion model.[49] The diffusion coefficient histogram was analyzed by a binominal distribution. Trajectories were separated by their diffusion coefficient. Slow diffusion coefficients were regarded as the single molecules in l_o domains, whereas fast diffusion coefficients were single molecules in l_d domains. After filtering by their diffusion coefficients, single molecules in the l_o and the l_d phase were counted and normalized to the given surface area (n_{l_o} and n_{l_d}, respectively). The ratio l_o/l_d was obtained by dividing the number of single molecules in the l_o phase and l_d phase. The ratio was obtained from three squares in three independent experiments:

$$l_o/l_d = \frac{n_{l_o}}{n_{l_d}} \quad (2)$$

Conflict of Interest: The authors declare no competing financial interest.

Supporting Information Available: The Supporting Information is available free of charge on the ACS Publications website at DOI: 10.1021/acsnano.5b02696.

Video showing triggered phase partitioning of ^{Cy5}MBP-H6 upon addition of anti-MBP IgG (AVI)
Video showing triggered phase partitioning of ^{DY647}EGFR-H6 upon addition of EGF (AVI)
Additional text describing materials and methods, 3 tables and 15 figures showing diverse control experiments, and derivation of the model quantitatively describing phase partitioning (PDF)

Acknowledgment. We thank G. Hikade and H. Kenneweg for technical support and A. Honigmann for fruitful discussions. The H6-tagged anti-GFP nanobody was kindly provided by U. Rothbauer, Tübingen, Germany. This project was supported by the Deutsche Forschungsgemeinschaft (Grant SFB 944 to J.P. and H.-J.S.; Grant TRR83 to Ü.C.) and by the German Federal Ministry of Education and Research grant to the German Center for Diabetes Research.

REFERENCES AND NOTES

1. Piehler, J. New Methodologies for Measuring Protein Interactions *in Vivo* and *in Vitro*. *Curr. Opin. Struct. Biol.* **2005**, *15*, 4–14.
2. Fields, S.; Song, O. A Novel Genetic System to Detect Protein-Protein Interactions. *Nature* **1989**, *340*, 245–6.
3. Bruckner, A.; Polge, C.; Lentze, N.; Auerbach, D.; Schlattner, U. Yeast Two-Hybrid, a Powerful Tool for Systems Biology. *Int. J. Mol. Sci.* **2009**, *10*, 2763–88.
4. Hu, C. D.; Chinenov, Y.; Kerppola, T. K. Visualization of Interactions among Bzip and Rel Family Proteins in Living Cells Using Bimolecular Fluorescence Complementation. *Mol. Cell* **2002**, *9*, 789–98.
5. Kodama, Y.; Hu, C. D. Bimolecular Fluorescence Complementation (Bifc): A 5-Year Update and Future Perspectives. *BioTechniques* **2012**, *53*, 285–98.
6. Remy, I.; Michnick, S. W. Application of Protein-Fragment Complementation Assays in Cell Biology. *BioTechniques* **2007**, *42*, 137–145.
7. Lowder, M. A.; Appelbaum, J. S.; Hobert, E. M.; Schepartz, A. Visualizing Protein Partnerships in Living Cells and Organisms. *Curr. Opin. Chem. Biol.* **2011**, *15*, 781–8.
8. MacBeath, G.; Schreiber, S. L. Printing Proteins as Microarrays for High-Throughput Function Determination. *Science* **2000**, *289*, 1760–3.
9. Uetz, P.; Giot, L.; Cagney, G.; Mansfield, T. A.; Judson, R. S.; Knight, J. R.; Lockshon, D.; Narayan, V.; Srinivasan, M.; Pochart, P.; et al. A Comprehensive Analysis of Protein-Protein Interactions in Saccharomyces Cerevisiae. *Nature* **2000**, *403*, 623–7.
10. LaBaer, J.; Ramachandran, N. Protein Microarrays as Tools for Functional Proteomics. *Curr. Opin. Chem. Biol.* **2005**, *9*, 14–9.
11. Lee, H. J.; Yan, Y.; Marriott, G.; Corn, R. M. Quantitative Functional Analysis of Protein Complexes on Surfaces. *J. Physiol.* **2005**, *563*, 61–71.
12. Wienken, C. J.; Baaske, P.; Rothbauer, U.; Braun, D.; Duhr, S. Protein-Binding Assays in Biological Liquids Using Microscale Thermophoresis. *Nat. Commun.* **2010**, *1*, 100.
13. Perozzo, R.; Folkers, G.; Scapozza, L. Thermodynamics of Protein-Ligand Interactions: History, Presence, and Future Aspects. *J. Recept. Signal Transduction Res.* **2004**, *24*, 1–52.
14. Chaires, J. B.; Hansen, L. D.; Keller, S.; Brautigam, C. A.; Zhao, H.; Schuck, P. Biocalorimetry. *Methods* **2015**, *76*, 1–2.
15. Schuck, P. Analytical Ultracentrifugation as a Tool for Studying Protein Interactions. *Biophys. Rev.* **2013**, *5*, 159–171.
16. Groves, J. T.; Boxer, S. G. Micropattern Formation in Supported Lipid Membranes. *Acc. Chem. Res.* **2002**, *35*, 149–57.
17. Chan, Y. H.; Boxer, S. G. Model Membrane Systems and Their Applications. *Curr. Opin. Chem. Biol.* **2007**, *11*, 581–7.
18. Liu, C.; Monson, C. F.; Yang, T.; Pace, H.; Cremer, P. S. Protein Separation by Electrophoretic-Electroosmotic Focusing on Supported Lipid Bilayers. *Anal. Chem.* **2011**, *83*, 7876–80.
19. Loew, M.; Springer, R.; Scolari, S.; Altenbrunn, F.; Seitz, O.; Liebscher, J.; Huster, D.; Herrmann, A.; Arbuzova, A. Lipid Domain Specific Recruitment of Lipophilic Nucleic Acids: A Key for Switchable Functionalization of Membranes. *J. Am. Chem. Soc.* **2010**, *132*, 16066–72.
20. Lata, S.; Reichel, A.; Brock, R.; Tampé, R.; Piehler, J. High-Affinity Adaptors for Switchable Recognition of Histidine-Tagged Proteins. *J. Am. Chem. Soc.* **2005**, *127*, 10205–15.
21. Beutel, O.; Nikolaus, J.; Birkholz, O.; You, C.; Schmidt, T.; Herrmann, A.; Piehler, J. High-Fidelity Protein Targeting into Membrane Lipid Microdomains in Living Cells. *Angew. Chem., Int. Ed.* **2014**, *53*, 1311–5.
22. Roder, F.; Birkholz, O.; Beutel, O.; Paterok, D.; Piehler, J. Spatial Organization of Lipid Phases in Micropatterned Polymer-Supported Membranes. *J. Am. Chem. Soc.* **2013**, *135*, 1189.
23. Zacharias, D. A.; Violin, J. D.; Newton, A. C.; Tsien, R. Y. Partitioning of Lipid-Modified Monomeric Gfps into Membrane Microdomains of Live Cells. *Science* **2002**, *296*, 913–6.
24. Los, G. V.; Encell, L. P.; McDougall, M. G.; Hartzell, D. D.; Karassina, N.; Zimprich, C.; Wood, M. G.; Learish, R.; Ohana, R. F.; Urh, M.; et al. Halotag: A Novel Protein Labeling Technology for Cell Imaging and Protein Analysis. *ACS Chem. Biol.* **2008**, *3*, 373–82.
25. Rothbauer, U.; Zolghadr, K.; Muyldermans, S.; Schepers, A.; Cardoso, M. C.; Leonhardt, H. A Versatile Nanotrap for Biochemical and Functional Studies with Fluorescent Fusion Proteins. *Mol. Cell. Proteomics* **2008**, *7*, 282–9.
26. Lamken, P.; Lata, S.; Gavutis, M.; Piehler, J. Ligand-Induced Assembling of the Type I Interferon Receptor on Supported Lipid Bilayers. *J. Mol. Biol.* **2004**, *341*, 303–18.
27. Roisman, L. C.; Jaitin, D.; Baker, D. P.; Schreiber, G. Mutational Analysis of the Ifnar1 Binding Site on Ifnalpha2 Reveals the Architecture of a Weak Ligand-Receptor Binding-Site. *J. Mol. Biol.* **2005**, *353*, 271–81.
28. Pan, M.; Kalie, E.; Scaglione, B. J.; Raveche, E. S.; Schreiber, G.; Langer, J. A. Mutation of the Ifnar-1 Receptor Binding Site of Human Ifn-Alpha2 Generates Type I Ifn Competitive Antagonists. *Biochemistry* **2008**, *47*, 12018–27.
29. Waichman, S.; Bhagawati, M.; Podoplelova, Y.; Reichel, A.; Brunk, A.; Paterok, D.; Piehler, J. Functional Immobilization and Patterning of Proteins by an Enzymatic Transfer Reaction. *Anal. Chem.* **2010**, *82*, 1478–85.
30. Gavutis, M.; Lata, S.; Lamken, P.; Müller, P.; Piehler, J. Lateral Ligand-Receptor Interactions on Membranes Probed by Simultaneous Fluorescence-Interference Detection. *Biophys. J.* **2005**, *88*, 4289–302.
31. Chatterjee-Kishore, M.; van den Akker, F.; Stark, G. R. Association of Stats with Relatives and Friends. *Trends Cell Biol.* **2000**, *10*, 106–11.
32. Wenta, N.; Strauss, H.; Meyer, S.; Vinkemeier, U. Tyrosine Phosphorylation Regulates the Partitioning of Stat1 between Different Dimer Conformations. *Proc. Natl. Acad. Sci. U. S. A.* **2008**, *105*, 9238–43.
33. Stancato, L. F.; David, M.; Carter-Su, C.; Larner, A. C.; Pratt, W. B. Preassociation of Stat1 with Stat2 and Stat3 in Separate Signalling Complexes Prior to Cytokine Stimulation. *J. Biol. Chem.* **1996**, *271*, 4134–4137.
34. Wedeking, T.; Lochte, S.; Richter, C. P.; Bhagawati, M.; Piehler, J.; You, C. Single Cell Gfp-Trap Reveals Stoichiometry and Dynamics of Cytosolic Protein Complexes. *Nano Lett.* **2015**, *15*, 3610–5.
35. Yarden, Y.; Sliwkowski, M. X. Untangling the Erbb Signalling Network. *Nat. Rev. Mol. Cell Biol.* **2001**, *2*, 127–37.
36. Zhang, X.; Gureasko, J.; Shen, K.; Cole, P. A.; Kuriyan, J. An Allosteric Mechanism for Activation of the Kinase Domain of Epidermal Growth Factor Receptor. *Cell* **2006**, *125*, 1137–49.
37. Jura, N.; Endres, N. F.; Engel, K.; Deindl, S.; Das, R.; Lamers, M. H.; Wemmer, D. E.; Zhang, X.; Kuriyan, J. Mechanism for Activation of the Egf Receptor Catalytic Domain by the Juxtamembrane Segment. *Cell* **2009**, *137*, 1293–307.
38. Endres, N. F.; Das, R.; Smith, A. W.; Arkhipov, A.; Kovacs, E.; Huang, Y.; Pelton, J. G.; Shan, Y.; Shaw, D. E.; Wemmer, D. E.; et al. Conformational Coupling across the Plasma Membrane in Activation of the Egf Receptor. *Cell* **2013**, *152*, 543–56.
39. Coskun, U.; Simons, K. Cell Membranes: The Lipid Perspective. *Structure* **2011**, *19*, 1543–8.
40. Miljan, E. A.; Meuillet, E. J.; Mania-Farnell, B.; George, D.; Yamamoto, H.; Simon, H. G.; Bremer, E. G. Interaction of the Extracellular Domain of the Epidermal Growth Factor Receptor with Gangliosides. *J. Biol. Chem.* **2002**, *277*, 10108–13.
41. Coskun, U.; Grzybek, M.; Drechsel, D.; Simons, K. Regulation of Human Egf Receptor by Lipids. *Proc. Natl. Acad. Sci. U. S. A.* **2011**, *108*, 9044–8.
42. Lemmon, M. A.; Bu, Z.; Ladbury, J. E.; Zhou, M.; Pinchasi, D.; Lax, I.; Engelman, D. M.; Schlessinger, J. Two Egf Molecules Contribute Additively to Stabilization of the Egfr Dimer. *EMBO J.* **1997**, *16*, 281–94.
43. Roder, F.; Waichman, S.; Paterok, D.; Schubert, R.; Richter, C.; Liedberg, B.; Piehler, J. Reconstitution of Membrane Proteins into Polymer-Supported Membranes for Probing

Diffusion and Interactions by Single Molecule Techniques. *Anal. Chem.* **2011**, *83*, 6792–9.
44. Johnson, S. A.; Stinson, B. M.; Go, M. S.; Carmona, L. M.; Reminick, J. I.; Fang, X.; Baumgart, T. Temperature-Dependent Phase Behavior and Protein Partitioning in Giant Plasma Membrane Vesicles. *Biochim. Biophys. Acta, Biomembr.* **2010**, *1798*, 1427–35.
45. Sezgin, E.; Levental, I.; Grzybek, M.; Schwarzmann, G.; Mueller, V.; Honigmann, A.; Belov, V. N.; Eggeling, C.; Coskun, U.; Simons, K.; et al. Partitioning, Diffusion, and Ligand Binding of Raft Lipid Analogs in Model and Cellular Plasma Membranes. *Biochim. Biophys. Acta, Biomembr.* **2012**, *1818*, 1777–1784.
46. Vogelsang, J.; Kasper, R.; Steinhauer, C.; Person, B.; Heilemann, M.; Sauer, M.; Tinnefeld, P. A Reducing and Oxidizing System Minimizes Photobleaching and Blinking of Fluorescent Dyes. *Angew. Chem., Int. Ed.* **2008**, *47*, 5465–9.
47. Serge, A.; Bertaux, N.; Rigneault, H.; Marguet, D. Dynamic Multiple-Target Tracing to Probe Spatiotemporal Cartography of Cell Membranes. *Nat. Methods* **2008**, *5*, 687–94.
48. Sander, J.; Ester, M.; Kriegel, H. P.; Xu, X. W. Density-Based Clustering in Spatial Databases: The Algorithm Gdbscan and Its Applications. *Data Min Knowl Discov* **1998**, *2*, 169–194.
49. Saxton, M. J.; Jacobson, K. Single-Particle Tracking: Applications to Membrane Dynamics. *Annu. Rev. Biophys. Biomol. Struct.* **1997**, *26*, 373–99.